Water Practice & Technology

IWA PUBLISHING

Water Practice & Technology Vol 18 No 9, 2068 doi: 10.2166/wpt.2023.131

Attapulgite as an eco-friendly adsorbent in the treatment of real radioactive wastewater

Wasan A. Muslim[a], Salam A. Al-Nasri[b], Talib M. Albayati [c,*] and Issam K. Salih[d]

[a] Iraqi Geological Survey/Ministry of Industry and Minerals, Baghdad, Iraq
[b] Iraqi Atomic Energy Commission (IAEC)/Radiation and Nuclear Safety Directorate, Baghdad, Iraq
[c] Department of Chemical Engineering, University of Technology – Iraq, 52 Alsinaa St., P.O. Box 35010, Baghdad, Iraq
[d] Department of Chemical Engineering and Petroleum Industries, Al-Mustaqbal University, Babylon 51001, Iraq
*Corresponding author. E-mail: Talib.M.Naieff@uotechnology.edu.iq

TMA, 0000-0001-5619-7760

ABSTRACT

Operators cannot ignore the radiation hazards arising from nuclear weapons. In this study, batch adsorption experiments were investigated to remove the radioactive isotope Cs-137 from the real radioactive wastewater. The attapulgite natural clay mineral was characterized and adopted as an adsorbent in a batch adsorption system. Equilibrium was reached after 2 h with a Cs-137 removal efficiency of 97% for attapulgite. The kinetics of Cs-137 adsorption on the attapulgite clay surface were evaluated. The pseudo-second-order kinetic model produced an excellent fit with the experimental kinetic data.

Key words: attapulgite, cesium adsorption, clay minerals, Cs-137, wastewater remediation

HIGHLIGHTS

- Very cheap attapulgite clay was used in a batch adsorption system.
- Iraqi attapulgite natural clay proved as an efficient adsorbent for the removal of Cs-137.
- Natural clay was modified and manufactured from a locally available material.
- The real samples of radioactive wastewater containing 137Cs have been treated.

GRAPHICAL ABSTRACT

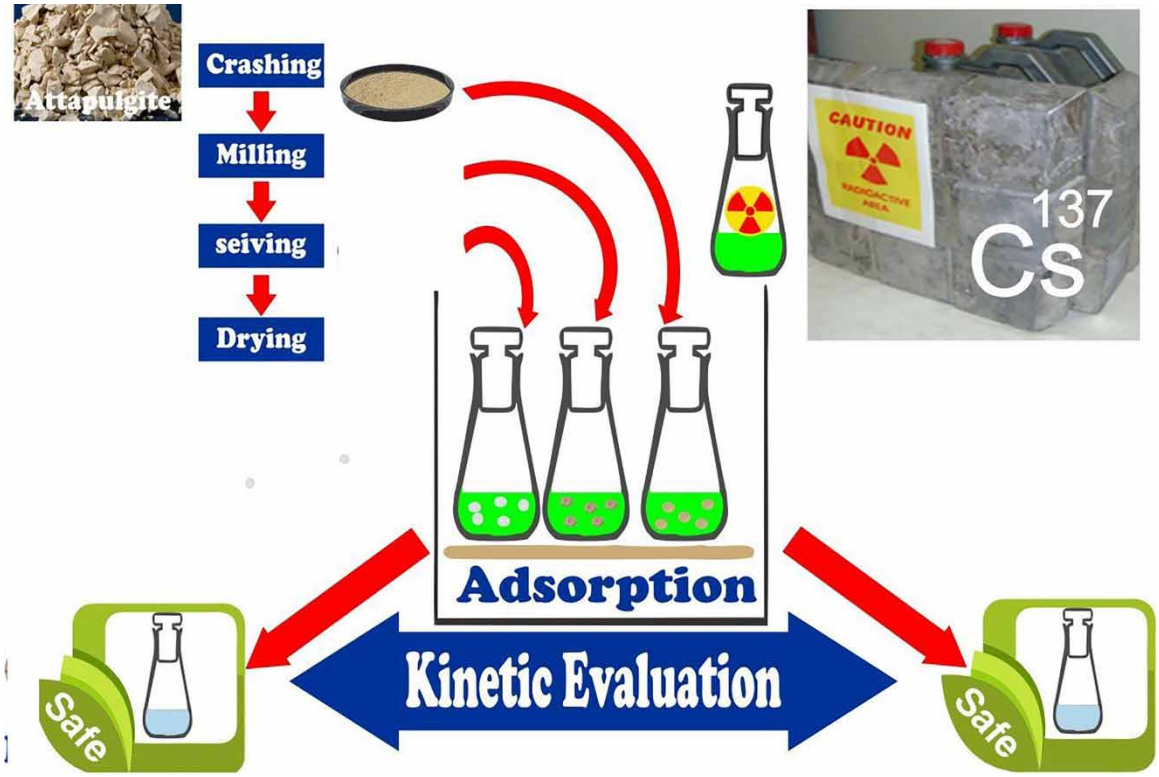

1. INTRODUCTION

Radioactive wastewater is one of the riskiest pollutants generated by energy stations, medical programs, and diverse extractive industries worldwide (Paranhos Gazineu *et al.* 2005). Effective treatments need to be cost-effective and safely reduce the volume of aqueous waste (International Atomic Energy Agency 2002; Cherif *et al.* 2017) containing long-lived beta/gamma activity stored in large tanks under nuclear sites. Cs-137 has a radioactive half-life of about 30 years and very high solubility in liquid systems, and incorporates into both the soil environment and aquatic organisms (Al-Alawy & Mzher 2019; Ahmed 2022). Liquids contaminated with Cs-137 are a potential environmental problem. High radioactivity aqueous wastes with long-lived radionuclides may be treated using different treatment technologies, including ion exchange/sorption, chemical precipitation, and/or evaporation, reverse osmosis, filtration, and solvent extraction (IAEA 1999). Many studies have found that adsorption is a good technique for removing radioactive materials from wastewater, with high activity and low operating cost (Alardhi *et al.* 2020; Kadhum *et al.* 2021; Ali *et al.* 2022a). The best media in the treatment of industrial wastewater were clay minerals whose features make them optimal adsorbents due to their low production cost, ready availability, non-toxic nature, high specific surfaces, excellent adsorption properties, and great potential for ion exchange (Al-Ani & Sarapää; 2008). Clay minerals adsorb cesium to balance the negative charge on the aluminosilicate structure caused by the counter-ions (e.g., Na, Ca, Mg, or K) as adsorption sites on the clay sheet surface, interlayers between sheets, and broken bonds at the edges of clay crystals (Wilson 2007; Yuan *et al.* 2013). Attapulgite is the rock name of palygorskite, a hydrated Mg–Al silicate material that has a 2:1 inverted structure, i.e., the apices of the silica tetrahedrons are regularly inverted along the *a*-axis. This results in parallel channels throughout the particles, which give these minerals a high internal specific surface containing exchangeable cations and water (Stewart & Mollins 1996). Large cation exchange capacities (CECs) and high total uptake of cesium occur when the interlayer sites are available for adsorption, as has been recorded in the cases of montmorillonite and palygorskite (Adebowale *et al.* 2006; Ohnuki & Kozai 2013; Okumura *et al.* 2013; Ali *et al.* 2022b). Several studies have inspected the mechanism of cesium adsorption by ion exchange with different potential sites on mineral surfaces and studied the effect of the structural characteristics of these clay minerals (Cornell 1993; Park *et al.* 2019; Zabulonov *et al.* 2021). Other research examined the parameters

that influence adsorption, adsorption isotherms, thermodynamics, and kinetics for many clay minerals (Sheha & Metwally 2007; Hadadi *et al.* 2009; Akalin *et al.* 2018; Semenkova *et al.* 2018; Muslim *et al.* 2022).

In this work, natural attapulgite clay minerals from the Western Desert of Iraq were selected as potential low-cost, readily available, environmentally friendly adsorbents adopted for use in a batch adsorption system. Attapulgite was implemented to treat real radioactive wastewater containing Cs-137 that has been accumulated since 1991 underneath the Al-Tuwaitha Nuclear Research Center near Baghdad, Iraq. The influence of various variables on the adsorption process was investigated along with its isotherms and kinetics.

2. EXPERIMENTAL WORK

2.1. Clay mineral preparation and characterization

Clays have characteristics that depend on their geological formation and mining location. Deposits of attapulgite occur in Wadi Bashira in Iraq's Western Desert. The representative sample was crushed in a jaw crusher (Retsch BB 1, Germany) and then milled in a rotating cylinder ball mill to pass a 75-μm sieve opening. Wet chemical analysis to identify the attapulgite's chemical composition was done in the Central Laboratories Department, Iraqi Geological Survey. X-ray diffraction (XRD) mineralogical analyses were performed using the Ital structure model MPD 3000 (Spain, Al Razi Metallurgical Center, Tehran, Iran). Scanning electron microscopy (SEM) and energy-dispersive X-ray spectroscopy (EDX) were employed to investigate clays' morphologies with the MIRA3 TESCAN instrument (Australia, Al Razi Metallurgical Center, Tehran, Iran). Particle size distribution analysis was done using a Brookhaven Instruments (USA) 90Plus particle size analyzer (Nanotechnology Center, UOT, Iraq). The minerals' specific surface area (SSA) and CECs were obtained from technical reports of the Iraqi Geological Survey (Baghdad, Iraq). Fourier-transform infrared (FT-IR) spectroscopy analyses were run with a Bomem MB-Series FT-IR Spectrometer (France) and operated according to ASTM E 1252-98(21) to specify the functional groups.

2.2. Radioactive wastewater sample preparation

The radioactive wastewater samples were taken from a reservoir underneath the destroyed Radiochemical Laboratories (RCL) at the Al-Tuwaitha site (Iraq). The gamma spectroscopy analysis was conducted using a closed-end, coaxial, p-type model (GEM65P4-95/ORTEC (USA, Al-Tuwaitha site, Iraq) high purity germanium detector (HPGe), yielding high-level waste (HLW) containing radioactive cesium (Cs-137) with a specific activity of 4.5 GBq/L (Ibrahim *et al.* 2018). As per the appropriate safety procedure, the sample was diluted with distilled water to a safe limit to be handled within the laboratory. The activity was reduced to about 6,372 Bq/L, which is considered the initial activity concentration.

2.3. Batch adsorption experiments

Batch mode experiments were carried out to evaluate the use of the clay to adsorb Cs-137 from the radioactive wastewater. In glass containers, 0.1 g of clay was added to 30 mL radioactive wastewater samples, with Cs-137 activity concentration of 6,372 Bq/L and pH 6. The sample containers were shaken at 200 rpm at room temperature (25 °C) for different mixing times (i.e., 0.5, 1, 1.5, 2, and 3 h). Solid particles were separated from the solution by centrifugation rather than filtration, using filter paper, to avoid the adsorption of contaminants onto the filter paper. Filtrate samples (20 mL) were put into a Marinelli beaker to measure the cesium radioactivity concentration after treatment using gamma spectroscopy (HPGe detector). The Cs-137 (μg/L) concentrations in the filtrates were estimated using Equations (1)–(4) (Knoll & Wegst 1980):

$$\text{Specific activity (SA)} = \frac{\lambda \times Aav \times w}{m} \tag{1}$$

$$w = \frac{\text{SA} \times m}{\lambda \times Aav} \tag{2}$$

where Aav is Avogadro's number (6.02×10^{23} nuclei/mol), λ is the radioisotope decay constant (s^{-1}), m is the atomic weight (g/mol), and w is the weight (g).

$$\lambda = \frac{\ln 2}{\text{half-life}} = \frac{0.693}{t^{1/2}} \tag{3}$$

$$\text{Cs isotope concentration in filtrate } (C) = \frac{w}{v} \tag{4}$$

The clay was investigated by studying the removal efficiency ($R\%$), adsorption capacity, q_e (mg/g), and adsorption coefficient, K_d (L/g), respectively, of the Cs-137 isotope at equilibrium, using Equations (5)–(7) (Abbood *et al.* 2022):

$$R\% = \frac{\text{concentration of adsorbed cesium}}{\text{initial concentration of cesium}} = \frac{C_0 - C_e}{C_0} \times 100 \quad (5)$$

$$q_e = \frac{\text{amount of cesium adsorbed}}{\text{amount of adsorbent}} = \frac{(C_0 - C_e) \times V}{M} \quad (6)$$

$$K_d = \frac{C_0 - C_e}{C_e} \times \frac{V}{M} = \frac{q_e}{C_e} \quad (7)$$

where C_0 and C_e are the initial and equilibrium concentrations of radioactive cesium (mg/L), V is the solution volume (L), and M is the weight of the clay mineral (g).

2.4. Adsorption kinetics

The Cs-137 adsorption mechanism on the clay surfaces was investigated using the contact time data. Three linearized adsorption kinetics models were used to evaluate the experimental results – pseudo-first-order (Lagergren model), pseudo-second-order (Ho model), and intraparticle diffusion (Weber–Morris model) – which are represented by Equations (8)–(10), respectively (Al-Jaaf *et al.* 2022; Jabbar *et al.* 2022):

$$\ln(q_e - q_t) = \ln q_e - k_1 t \quad (8)$$

$$\frac{t}{q_t} = \frac{1}{k_2 q_e^2} + \frac{t}{q_e} \quad (9)$$

$$q_t = K_P t^{1/2} + C \quad (10)$$

where q_e and q_t are the adsorption capacity (mg/g) at equilibrium and time t (min), respectively; K_1 and K_2 are adsorption rate constants of the pseudo-first-order (min^{-1}) and pseudo-second-order (g/mg·min), respectively; K_P is the intraparticle diffusion rate ($mg/g{\cdot}min^{0.5}$) constant, and C is the diffusion intraparticle constant (Khadim *et al.* 2022).

3. RESULTS AND DISCUSSION

3.1. Clay mineral characterization

The results of the chemical and mineralogical analyses of the attapulgite are shown in Table 1 and Figure 1.

Table 1 | Chemical analyses of the clays

Chemical composition	SiO_2b (%)	Al_2O_3 (%)	Fe_2O_3 (%)	CaO (%)	MgO (%)	SO_3 (%)	LOI (%)	Na_2O (%)	K_2O (%)	Cl (%)
Attapulgite	40.1	9.6	3.38	19.64	4.36	0.32	20.5	0.8	0.29	

LOI, loss on ignition.

The attapulgite sample contains predominantly montmorillonite (smectite) associated with palygorskite as the main minerals, in addition to impurities like silica, calcite, and gypsum, as shown in Table 1 (Al-Ajeel *et al.* 2008). The montmorillonite is considered a Ca-montmorillonite on the basis of the ratio of ($Na_2O + K_2O$) to ($CaO +$ MgO), which is approaching 0.136 (Abdou *et al.* 2013).

In Figure 1, the XRD analyses illuminate a convergence for attapulgite, in which the major peaks are palygorskite at 20° and 8° diffraction angles (2θ), and the minor mineral is montmorillonite with 2θ at 20.5° and 7°. In fact, the sample is a montmorillonite-rich, palygorskite clay. The results show clearly that the clays have not been subject to any purification or modification processes.

Figure 2 displays the SEM images for the attapulgite clay. As can be seen, the original attapulgite structure consisted of blocks, channels, and 'ribbon-like' sheets, while after adsorption, the framework collapsed with the disorder in the layered structure, and the particles were almost flat (Muslim *et al.* 2022).

EDX qualitative elemental composition analysis, by identifying the material's crystal structure, was achieved at 'a' in Figure 2, after adsorption on the attapulgite clay surface. The EDX results are shown in Figure 3.

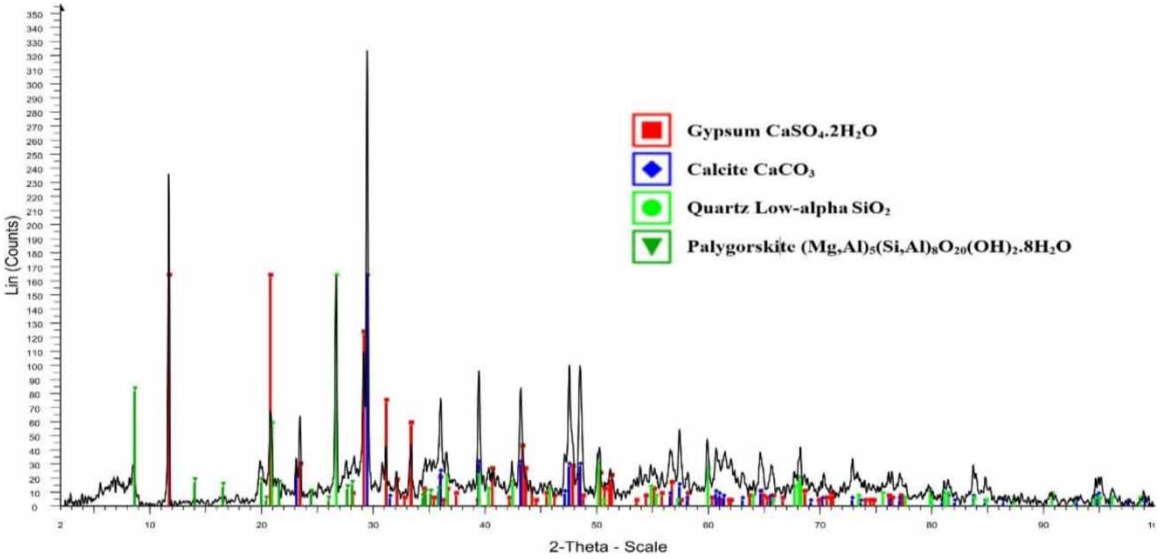

Figure 1 | XRD patterns of attapulgite.

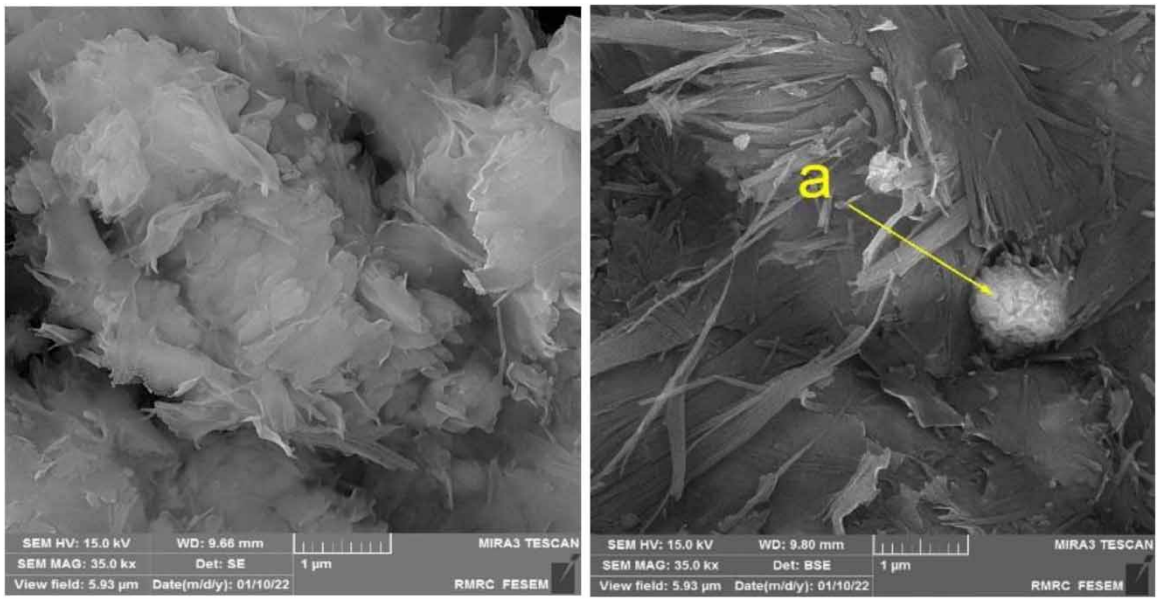

Figure 2 | SEM images for attapulgite. 'a' represents a known point on the clay surface analyzed after adsorption.

The EDX spectrum detects the attapulgite clay surfaces after adsorption and the presence of Cs-137 of the radioactive wastewater, as shown in Figure 3. The particle size test was based on dynamic light scattering (DLS), and the clay's mean particle size is presented in Figure 4.

According to the particle size analysis, attapulgite exhibited small particle size. The surface areas were measured using the Brunauer, Emmett and Teller (BET) method. Attapulgite's specific surface and cation exchange capacity are given in Table 2.

The infrared spectra for attapulgite are shown in Figure 5. The spectrum after adsorption (Ab) shows the stretching vibration of Al–OH–Al, Mg–OH, and/or H_2O at 3,427 cm^{-1} and the stretching vibration of Si–O at 1,104 cm^{-1}, while the Si–OH stretching vibration appeared at 1,029 cm^{-1}. Moreover, the spectrum showed the stretching vibration bands of Si–O–Si and Si-–O–Al at 767 and 778 cm^{-1}. The change in the spectra appeared clearly when compared to the reading before the reaction, as shown in the spectrum before adsorption (Aa), with a solid shift in the vibration of Si–O, Si–OH, and Si–O–Si, which appeared at 1,104, 1,026, and 870/772 cm^{-1} (Muslim *et al.* 2022).

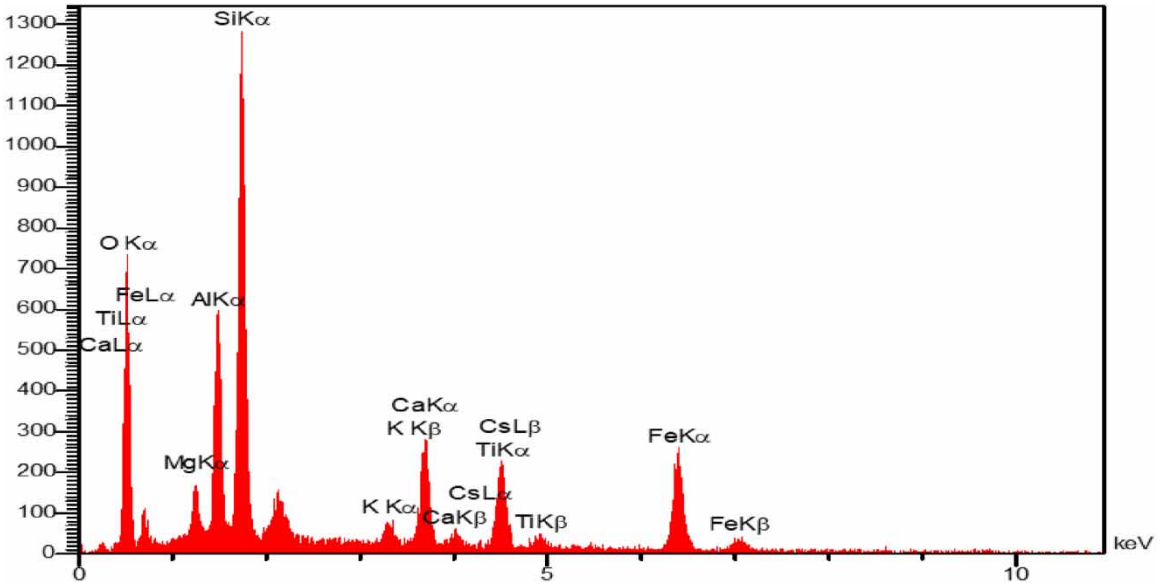

Figure 3 | EDX analysis of the attapulgite clay after adsorption.

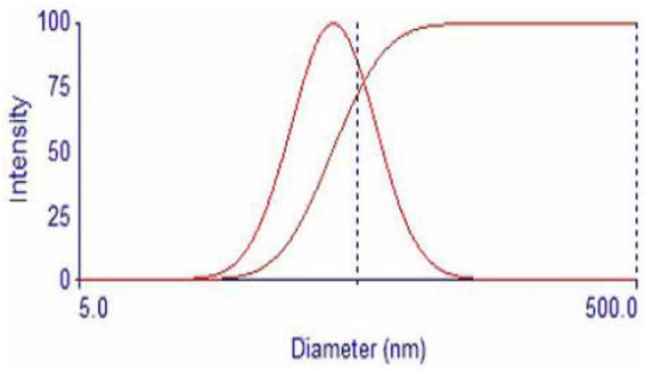

Figure 4 | Particle size analysis for attapulgite.

Table 2 | Mean particle size and specific surface of attapulgite

Sample	Mean particle diameter (nm)	St. Deviation	Density (g/cm^3)	CEC (meq/100 g)	SSA (m^2/g)
A	41.2	1.42	2.4	14.08	60.7

3.2. Batch adsorption results

3.2.1. Activity concentration and removal (%)

The results of the batch adsorption experiments are shown in Figure 6(a). The maximum reduction in Cs-137 activity was achieved at 177 Bq/L during the 2 h required for cesium uptake to reach equilibrium for attapulgite. The proportional removal (%) was determined using Equation (5) and is presented in Figure 6(b), which shows that equilibrium was reached quickly, achieving 80% adsorption after 1 h. However, at an equilibrium time of 2 h, attapulgite removal efficiency reached 97%. The montmorillonite (smectite) content in attapulgite, as shown in Figure 1, leads, firstly, to the reduction in attapulgite particle size. Also, attapulgite has high CEC, which represents the existence of active adsorption sites (Table 2). Secondly, montmorillonite's existence in attapulgite causes the absorption of a significant amount of water (expandable clays), making the process a combination of absorption and adsorption (called sorption), which boosted cesium uptake from the wastewater (Park *et al.* 2019).

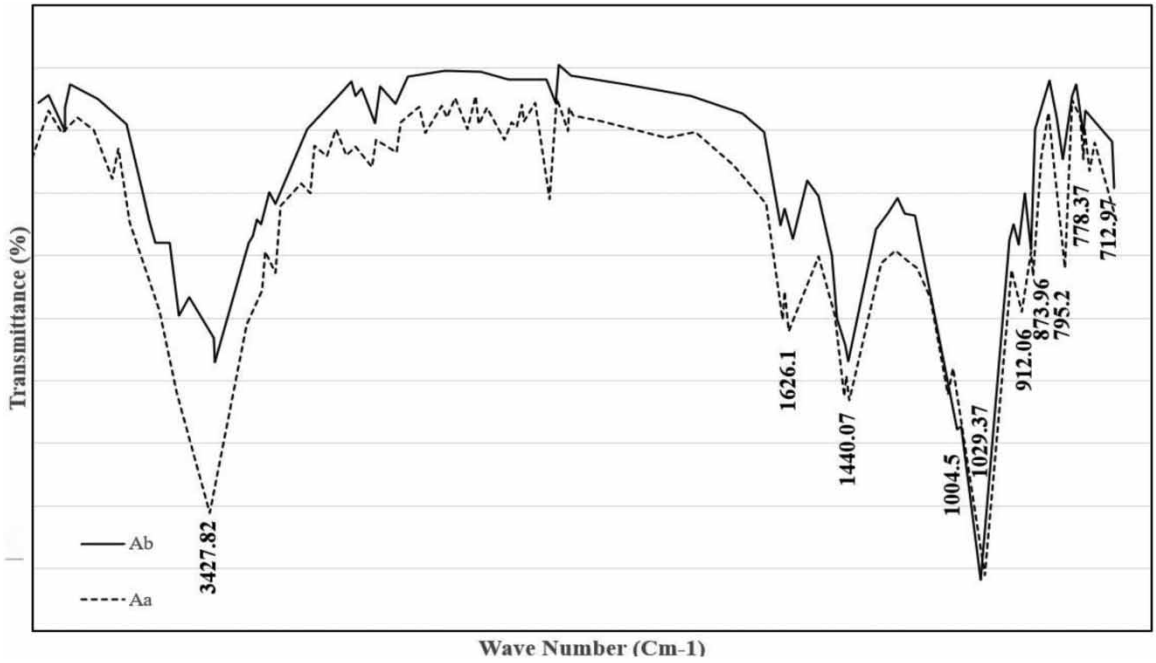

Figure 5 | FT-IR spectra of attapulgite (Ab) before adsorption and (Aa) after adsorption.

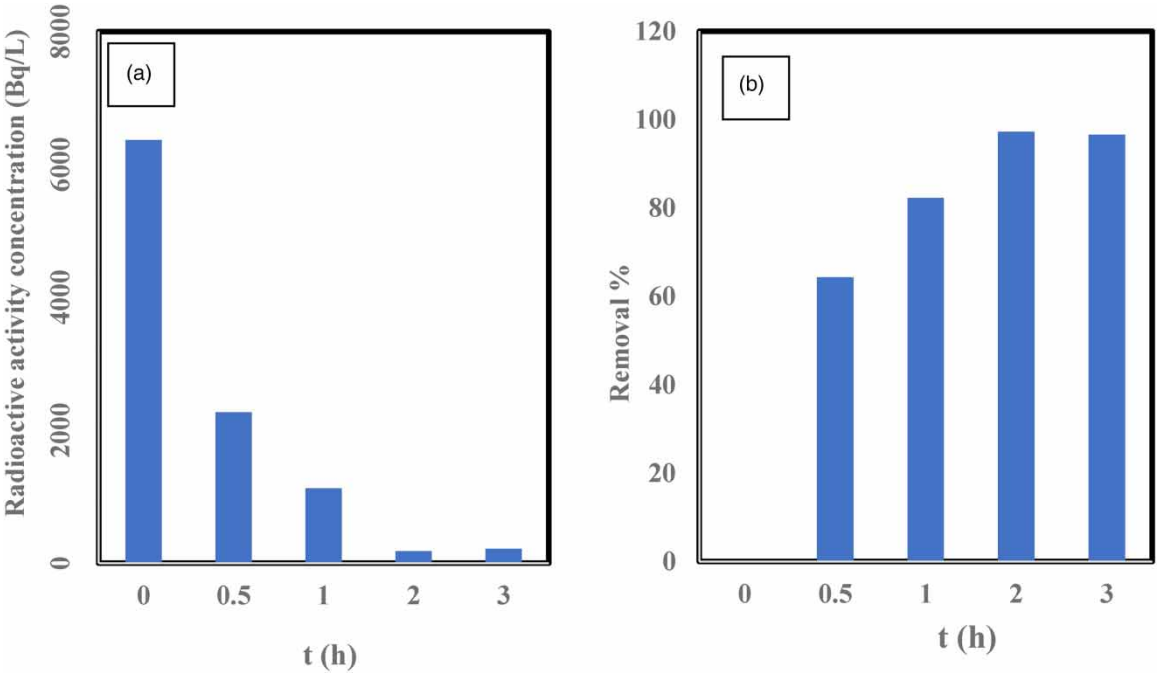

Figure 6 | Effect of contact time on (a) activity concentration and (b) removal (%) of Cs-137 from radioactive wastewater for attapulgite.

3.2.2. Mechanisms of Cs sorption

The extent of Cs adsorption on montmorillonite and attapulgite depends on the minerals' ion exchange site types, which is characterized by the function and availability of the interlayer site type (III) that offers high CECs and cesium uptake. In attapulgite, the active sites are only in the planar (basal) surface (type I) and the edges of the interlayers (type II), which both show low CECs compared to type III. In kaolinite, the ion exchange capability is due to broken bonds at the edges of the clay plates and hydroxyl groups on the basal lamellar. The results indicate

that Cs is adsorbed not only at the 'frayed edge' sites but also at other sites where the adsorption is reversible, as reported by Erten *et al.* (1988), Comans *et al.* (1991), Comans & Hockley (1992), and Shahwan *et al.* (1999). One is instantaneous and reversible on a timescale of a few days or less. The other is irreversible, occurs at longer times, and is caused by Cs migration into the interlayers. Slow Cs migration into interlayers was also proposed by Evans *et al.* (1983). These were in accord with the extent of cesium adsorption (desorption) by attapulgite after 2 h in the results as clarified in Figure 6(b), because some of the cesium sites are reversible on attapulgite's basal planes. The results of this study are agreement with the mechanism of adsorption (Ali *et al.* 2023; Khader *et al.* 2023).

3.2.3. Adsorption capacity and distribution coefficient

The adsorption capacity (q_e) and distribution coefficient (K_d) for the attapulgite at different contact times were calculated from Equations (6) and (7), respectively, and are shown in Figure 7(a) and 7(b), respectively. Clearly, the prime K_d and q_e for attapulgite after 2 h of contact time were caused by the very low initial Cs-137 concentration, because sorption increased sharply then (Missana *et al.* 2014; Baborová *et al.* 2018).

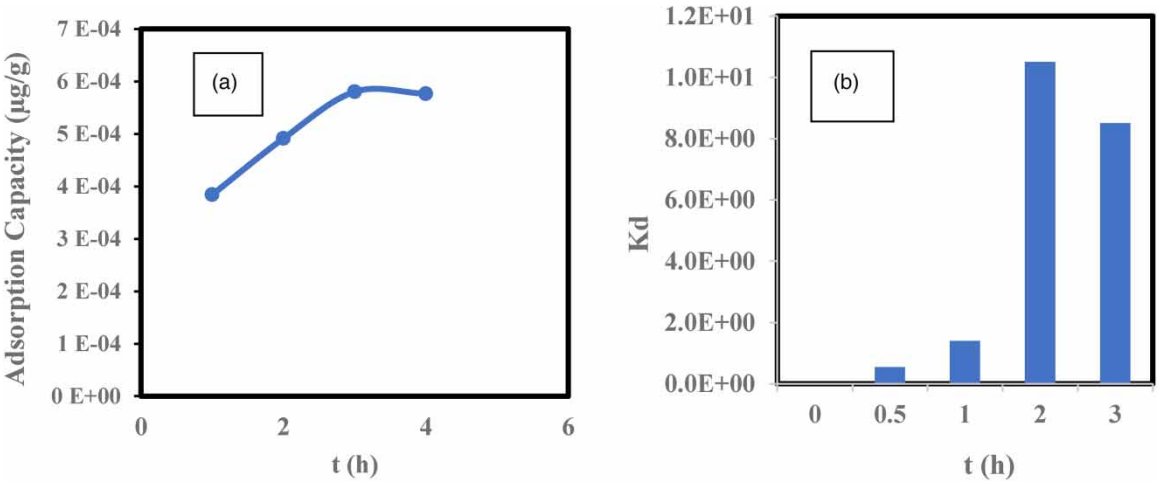

Figure 7 | (a) Adsorption capacity (q_e) and (b) adsorption distribution coefficient (K_d) for attapulgite.

3.3. Adsorption kinetics

The results from the kinetic models for attapulgite – pseudo-first-order (Equation (8)), pseudo-second-order (Equation (9)), and intraparticle diffusion (Equation (10)) – are displayed in Figure 8(a)–8(c), respectively. The Cs-137 adsorption mechanisms for attapulgite better fit the pseudo-second-order kinetic model with a high regression coefficient of 0.9971, which is higher than the pseudo-first-order model value of 0.9919.

The q_e predicted for attapulgite by the pseudo-first-order model approached the experimental q_e, as shown in Table 3. The intraparticle diffusion adsorption kinetic model is based on the assumption that the rate-controlling step may involve valence forces through ion exchange, substitution, or complexation (Wei *et al.* 2019; Al-Rahmani *et al.* 2020).

Since the plot of q_t versus $t^{(0.5)}$ in the intraparticle model, as shown in Figure 8(c), did not pass the origin, intraparticle diffusion did not wholly affect the adsorption process. Also, the diffusion model's correlation coefficient (R^2) for attapulgite was lower than that of the pseudo-second-order (0.867), as shown in Table 3. The suitability of the pseudo-second-order model with the experimental result means that adsorption is controlled by ion exchange, in which electrostatic interactions play a significant part (Jiaojiao *et al.* 2009; Xiang *et al.* 2014).

3.4. Comparative study

The research focus is the exploration of novel and effective adsorbents for Cs removal. The widespread exploration of advanced functional materials for nuclide pollution control is driven by increasingly severe environmental problems. Researchers have extensively explored and designed adsorbents for Cs removal. A comparison between the results of this study and previous studies is illustrated in Table 4 and suggests that attapulgite is a

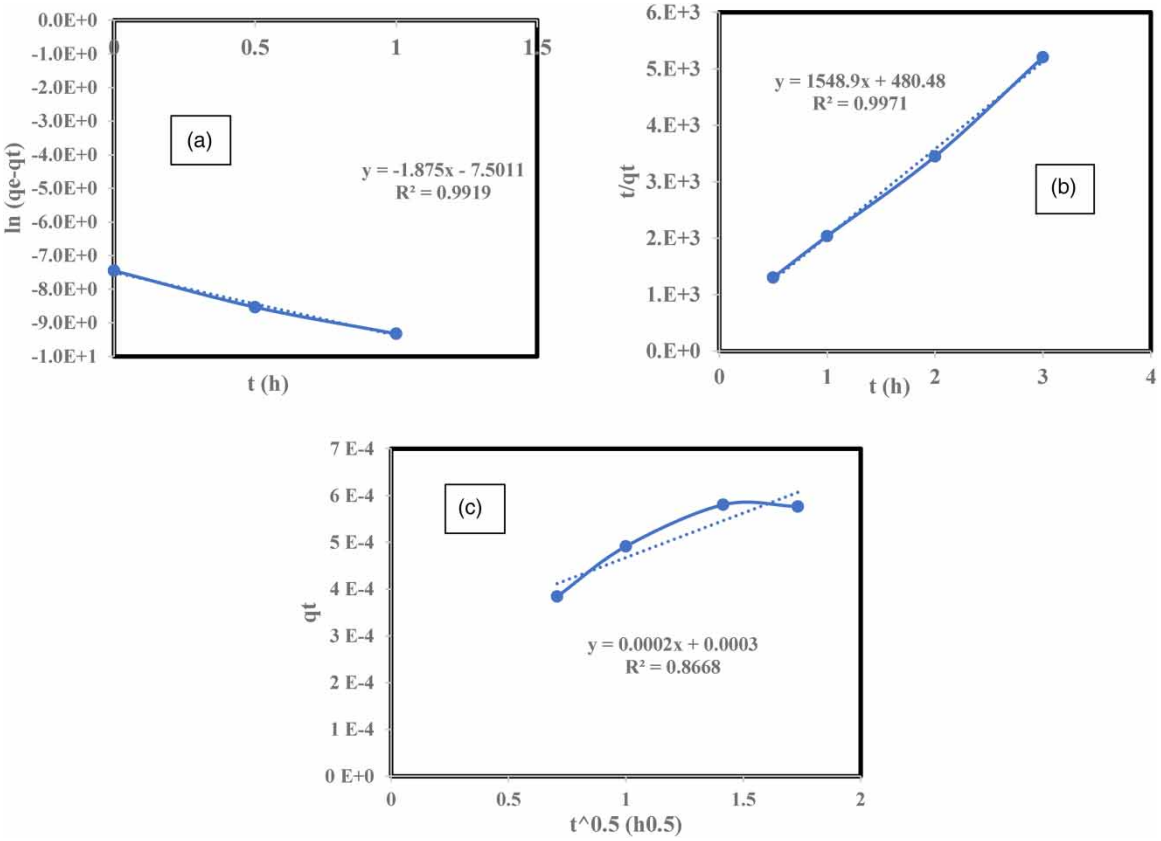

Figure 8 | Adsorption kinetic models of attapulgite: (a) pseudo-first-order adsorption kinetic model, (b) pseudo-second-order adsorption kinetic model, and (c) intraparticle diffusion model.

Table 3 | Kinetic model adsorption parameters for attapulgite

	Experimental	Pseudo-first-order model		Pseudo-second-order model		Intraparticle diffusion model	
	q_e (mg/g)	q_e (mg/g)	R^2	q_e (mg/g)	R^2	C (mg/g)	R^2
Attapulgite	0.58×10^{-6}	0.55×10^{-6}	0.991	0.45×10^{-6}	0.9971	0.3	0.867

Table 4 | Adsorption capacities and removal efficiency of Cs-137 by various adsorbents

Adsorbents	Adsorption capacity Q_{max} (mg/g)	Removal efficiency (%)	Equilibrium time (h)	References
Nanoclusters microparticles	45.87	99.7	6	Yang *et al.* (2016)
Nanocomposites with graphene oxide	55.56	90	12	Yang *et al.* (2014)
Nanoparticles	96.00	NA	24	Thammawong *et al.* (2013)
Nanocomposites	280.82	NA	24	Jang & Lee (2016)
Nanoparticles with PEG	274.70	64.8	1	Qian *et al.* (2017)
Microparticles	16.30	97.0	10 min	Wang *et al.* (2020)
Attapulgite	NA	97	2	This study

strong, stable, and efficient sorbent for Cs-137 removal. Moreover, attapulgite is easily applied as an adsorbent with a natural, low-cost, eco-friendly, and simple batch sorption process compared with synthesized adsorbents, such as zeolites, composites, and bio-sorbents for Cs-137 radioactive decontamination. Excellent Cs-137

adsorption efficiencies were achieved by attapulgite (97%) for a 2-h equilibrium time without functionalization or treatment of its surface.

4. CONCLUSIONS

Attapulgite had a small particle size, a high specific surface, better cation exchangeability, and an effective functional site. Excellent adsorption efficiencies of Cs-137 were achieved by attapulgite (97%) for a 2-h equilibrium time. The high adsorption efficiencies achieved in this study resulted from using low Cs-137 radioactivity concentrations (~6.372 KBq/L). The kinetics of Cs-137 adsorption on attapulgite were evaluated. The pseudo-second-order kinetic model produces a good fit with the experimental data. According to the results, the local raw attapulgite was suitable clay and should be selected to manage the removal of the Cs-137 from wastewater. The attapulgite adsorbents proved to be promising materials for removing Cs-137 because they are inexpensive, available, and effective.

ACKNOWLEDGEMENTS

We gratefully acknowledge the scientific support of the Department of Chemical Engineering, University of Technology-Iraq; Iraqi Atomic Energy Commission (IAEC)/Radiation and Nuclear Safety Directorate, Baghdad, Iraq, and the Iraqi Geological Survey/Ministry of Industry and Minerals, and the Department of Chemical and Petroleum Industries Engineering at Al-Mustaqbal University College in Babylon, Iraq.

DATA AVAILABILITY STATEMENT

All relevant data are included in the paper or its Supplementary Information.

CONFLICT OF INTEREST

The authors declare there is no conflict.

REFERENCES

Abbood, N. S., Ali, N. S., Khader, E. H., Majdi, H. S., Albayati, T. M. & Cata Saady, N. M. 2022 Photocatalytic degradation of cefotaxime pharmaceutical compounds onto a modified nanocatalyst. *Research on Chemical Intermediates*. https://doi.org/10.1007/s11164-022-04879-3.

Abdou, M. I., Al-sabagh, A. M. & Dardir, M. M. 2013 Evaluation of Egyptian bentonite and nano-bentonite as drilling mud. *Egyptian Journal of Petroleum* **22**(1), 53–59. doi:10.1016/j.ejpe.2012.07.002.

Adebowale, K. O., Unuabonah, I. E. & Olu-Owolabi, B. I. 2006 The effect of some operating variables on the adsorption of lead and cadmium ions on kaolinite clay. *Journal of Hazardous Materials* **134**(1–3), 130–139. doi:10.1016/j.jhazmat.2005.10.056.

Ahmed, B. A. 2022 *Radiological Impact on Public Environment, and Risk Assessment Associated with Decommissioning of the Iraq Destroyed IRT-5000 Research Reactor*. https://doi.org/10.34726/hss.2022.27941.

Akalin, H. A., Hiçsönmez, U. & Yilmaz, H. 2018 Removal of cesium from aqueous solution by adsorption onto sivas-yildizeli (Türkiye) vermiculite: Equilibrium, kinetic and thermodynamic studies. *Journal of the Turkish Chemical Society, Section A: Chemistry* **5**(1), 85–116. doi:10.18596/jotcsa.317771.

Al-Ajeel, A. A., Abdullah, N. S. & Mustafa, A. M. 2008 Beneficiation of attapulgite- montmorillonite claystone by dispersion sedimentation. *Iraqi Bulletin of Geology and Mining* **4**(1), 117–124.

Al-Alawy, I. T. & Mzher, O. A. 2019 Radiological characterization of the irt-5000(14-Tammuz) research nuclear reactor at Al-Tuwaitha nuclear center in Iraq. *Environmental Earth Sciences* **78**(6), 1–9. doi:10.1007/s12665-019-8122-6.

Al-Ani, T. & Sarapää, O. 2008 Clay and clay mineralogy. In: *Geochemical Survey of Finland*, M19/3232/2008/41. Espoo, Finland, pp. 1–94.

Alardhi, S. M., Alrubaye, J. M. & Albayati, T. M. 2020 Removal of methyl green dye from simulated waste water using hollow fiber ultrafiltration membrane. In *2nd International Scientific Conference of Al-Ayen University (ISCAU-2020), IOP Conf. Series: Materials Science and Engineering*, Vol. 928, p. 052020. doi:10.1088/1757-899X/928/5/052020.

Ali, N. S., Jabbar, N. M., Alardhi, S. M., Majdi, H. S. & Albayati, T. M. 2022a Adsorption of methyl violet dye onto a prepared bio-adsorbent from date seeds: Isotherm, kinetics, and thermodynamic studies. *Heliyon* **8**, e10276. https://doi.org/10.1016/j.heliyon.2022.e10276.

Ali, N. S., Kalash, K. R., Ahmed, A. N. & Albayati, T. M. 2022b Performance of a solar photocatalysis reactor as pretreatment for wastewater via UV, UV/TiO_2, and UV/H_2O_2 to control membrane fouling. *Scientific Reports* **12**, 16782. https://doi.org/10.1038/s41598-022-20984-0.

Ali, N. S., Harharah, H. N., Salih, I. K., Cata Saady, N. M., Zendehboudi, S. & Albayati, T. M. 2023 Applying MCM-48 mesoporous material, equilibrium, isotherm, and mechanism for the effective adsorption of 4-nitroaniline from wastewater. *Scientific Reports* **13**, 9837. https://doi.org/10.1038/s41598-023-37090-4.

Al-Jaaf, H. J., Ali, N. S., Alardhi, S. M. & Albayati, T. M. 2022 Implementing eggplant peels as an efficient bio-adsorbent for treatment of oily domestic wastewater. *Desalination and Water Treatment* **245**, 226–237. https://doi:.10.5004/dwt.2022.27986.

Al-Rahmani, A. A., Al-Attafi, S. K., Al-Nasri, S. K. & Jasim, Z. W. 2020 Hierarchical structures incorporating carbon and zeolite to remove radioactive contamination. *Iraqi Journal of Science* 1944–1951. Available form: https://ijs.uobaghdad.edu.iq/index.php/eijs/article/view/1320.

Baborová, L., Vopálka, D. & Červinka, R. 2018 Sorption of Sr and Cs onto Czech natural bentonite: Experiments and modelling. *Journal of Radioanalytical and Nuclear Chemistry* **318**, 2257–2262.

Cherif, M. A., Martin-Garin, A., Gérard, F. & Bildstein, O. 2017 A robust and parsimonious model for cesium sorption on clay minerals and natural clay materials. *Applied Geochemistry* **87**(October), 22–37. doi:10.1016/j.apgeochem.2017.10.017.

Comans, R. N. J. & Hockley, D. E. 1992 Kinetics of Cs sorption on illite. *Geochimica et Cosmochimica Acta* **56**, 1157–1164.

Comans, R. N. J., Hailer, M. & De Preter, P. 1991 Sorption of adsorption of Cs on kaolin & and illite 4073 Cs on illite: Nonequilibrium behavior and reversibility. *Geochimica et Cosmochimica Acta* **55**, 433–440.

Cornell, R. M. 1993 Adsorption of cesium on minerals: A review. *Journal of Radioanalytical and Nuclear Chemistry Articles* **171**(2), 483–500. doi:10.1007/BF02219872.

Erten, H. N., Aksoyoglu, S., Hatipoglu, S. & Göktürk, H. 1988 Sorption of cesium and strontium on montmorillonite and kaolinite. *Radiochim Acta* **44–45**(1), 147–152. doi:10.1524/ract.1988.4445.1.147.

Evans, D. W., Alberts, J. J. & Clark, R. A. 1983 Reversible ion exchange fixation of cesium-137 leading to mobilization from reservoir sediments. *Geochimica et Cosmochimica Acta* **47**, 1041–1049.

Hadadi, N., Kananpanah, S. & Abolghasemi, H. 2009 Equilibrium and thermodynamic studies of cesium adsorption on natural vermiculite and optimization of operation conditions. *Iranian Journal of Chemistry & Chemical Engineering* **28**(4), 29–36.

IAEA 1999 *Review of the Factors Affecting the Selection and Implementation of Waste Management Technologies; IAEA-TECDOC-1096*. IAEA, Vienna, Austria.

IAEA 2002 *Management of Low and Intermediate Level Radioactive Wastes with Regard to Their Chemical Toxicity*. International Atomic Energy Agency. Available from: https://www-pub.iaea.org/MTCD/publications/PDF/te_1325_web.pdf.

Ibrahim, Z. H., Mkhaiber, A. F. & Al-Nasri, S. K. 2018 *Estimation and Reduction of the Total Activity for the Liquid Waste Pool in Radiochemistry Laboratories in Al-Tuwaitha Site*. University of Baghdad, Baghdad.

Jabbar, N. M., Alardhi, S. M., Mohammed, A. K., Salih, I. K. & Albayati, T. M. 2022 Challenges in the implementation of bioremediation processes in petroleum-contaminated soils: A review. *Environmental Nanotechnology, Monitoring & Management* **18**, 100694. https://doi.org/10.1016/j.enmm.2022.100694.

Jang, J. & Lee, D. S. 2016 Magnetic Prussian blue nanocomposites for effective cesium removal from aqueous solution. *Industrial and Engineering Chemistry Research* **55**, 3852–3860.

Jiaojiao, W., Bing, L., Jiali, L., Yue, F., Dong, Z., Jun, Z., Wei, W., Yuanyou, Y. & Ning, L. 2009 Behavior, and analysis of cesium adsorption on montmorillonite mineral. *Journal of Environmental Radioactivity* **100**(10), 914–920. https://doi.org/10.1016/j.jenvrad.2009.06.024.

Kadhum, S. T., Alkindi, G. Y. & Albayati, T. M. 2021 Determination of chemical oxygen demand for phenolic compounds from oil refinery wastewater implementing different methods. *Desalination and Water Treatment* **231**, 44–53. doi:10.5004/dwt.2021.27443.

Khader, E. H., Khudhur, R. H., Abbood, N. S. & Albayati, T. M. 2023 Decolourisation of anionic azo dye in industrial wastewater using adsorption process: Investigating operating parameters. *Environmental Processes* **10**, 34. https://doi.org/10.1007/s40710-023-00646-7.

Khadim, A. T., Albayati, T. M. & Cata Saady, N. M. 2022 Removal of sulfur compounds from real diesel fuel employing the encapsulated mesoporous material adsorbent Co/MCM-41 in a fixed-bed column. *Microporous and Mesoporous Materials* **341**, 112020. https://doi.org/10.1016/j.micromeso.2022.112020.

Knoll, G. F. & Wegst, A. V. 1980 Radiation detection and measurement. *Medical Physics* **7**(4), 397–398. doi:10.1118/1.594739.

Missana, T., Benedicto, A., García-Gutiérrez, M. & Alonso, U. 2014 Modeling cesium retention onto Na-, K- and Ca-smectite: effects of ionic strength, exchange and competing cations on the determination of selectivity coefficients. *Geochim Cosmochim Acta* **128**, 266–277. doi:10.1016/j.gca.2013.10.007.

Muslim, W. A., Albayati, T. M. & Al-Nasri, S. K. 2022 Decontamination of actual radioactive wastewater containing Cs using bentonite as a natural adsorbent: Equilibrium, kinetics, and thermodynamic studies. *Science Reports* 1–12. doi:10.1038/s41598-022-18202-y.

Ohnuki, T. & Kozai, N. 2013 Adsorption behavior of radioactive cesium by non-mica minerals. *Journal of Nuclear Science and Technology* **50**(4), 369–375. doi:10.1080/00223131.2013.773164.

Okumura, M., Nakamura, H. & Machida, M. 2013 Mechanism of strong affinity of clay minerals to radioactive cesium: First-principles calculation study for adsorption of cesium at frayed edge sites in muscovite. *Journal of the Physical Society of Japan* **82**(3), 1–5. doi:10.7566/JPSJ.82.033802.

Paranhos Gazineu, M. H., de Araújo, A. A., Brandão, Y. B., Hazin, C. A. & de O Godoy, J. M. 2005 Radioactivity concentration in liquid and solid phases of scale and sludge generated in the petroleum industry. *Journal of Environmental Radioactivity* **81**(1), 47–54. https://doi.org/10.1016/j.jenvrad.2004.11.003.

Park, S. M., Lee, J., Jeon, E. K., Kang, S., Alam, M. S., Tsang, D. C. W., Daniel, S. A. & Kitae, B. 2019 , adsorption characteristics of cesium on the clay minerals: Structural change under wetting and drying condition. *Geoderma* **340**, 49–54. https://doi.org/10.1016/j.geoderma.2018.12.002.

Qian, J., Xu, J. Y., Kuang, L. J. & Hua, D. B. 2017 Cesium removal from human blood by poly(ethylene glycol)-decorated Prussian blue magnetic nanoparticles. *Chempluschem* **82**, 888–895.

Semenkova, A. S., Evsiunina, M. V., Verma, P. K., Mohapatra, P. K., Petrov, V. G., Seregina, I. F., Bolshov, M. A., Krupskaya, V. V., Romanchuk, A. Y. & Kalmykov, S. N. 2018 Cs+ sorption onto Kutch clays: influence of competing ions. *Applied Clay Science* **166**(September), 88–93. doi:10.1016/j.clay.2018.09.010.

Shahwan, T., Erten, H. N., Black, L. & Allen, G. C. 1999 TO-SIMS study of Cs+ sorption on natural 647 kaolinite. *The Science of the Total Environment* **226**(2–3), 255–260.

Sheha, R. R. & Metwally, E. 2007 Equilibrium isotherm modeling of cesium adsorption onto magnetic materials. *Journal of Hazardous Materials* **143**(1–2), 354–361. doi:10.1016/j.jhazmat.2006.09.041.

Stewart, D. I. & Mollins, L. H. 1996 Predicting the properties of bentonite-sand mixtures. *Clay Minerals* **31**(2), 243–252.

Thammawong, C., Opaprakasit, P., Tangboriboonrat, P. & Sreearunothai, P. 2013 Prussian blue-coated magnetic nanoparticles for removal of cesium from contaminated environment. *Journal of Nanoparticle Research* **15**, 10.

Wang, P. F., Zheng, J. L., Ma, X. L., Du, X., Gao, F. F., Hao, X. G., Tang, B., Abudula, A. & Guan, G. 2020 Electroactive magnetic microparticles for the selective elimination of cesium ions in the wastewater. *Environmental Research* **2020**(185), 9.

Wei, X., Sun, Y., Pan, D., Niu, Z., Xu, Z., Jiang, Y., Wu, W., Li, Z., Zhang, L. & Fan, Q. 2019 Adsorption properties of Na-palygorskite for Cs sequestration: Effect of pH, ionic strength, humic acid and temperature. *Applied Clay Science* **183**(April). doi:10.1016/j.clay.2019.105363.

Wilson, I. 2007 Applied Clay Mineralogy. occurrences, processing, and application of kaolin palygorskite sepiolite, and common clays. **55**, 6. doi:10.1007/bf03406033.

Xiang, L., Guan-Ru, C., Duu-Jong, L., Tohru, K., Hisashi, T., Man-Li, C. & Yu-Kuo, L. 2014 Adsorption removal of cesium from drinking waters: A mini-review on use of bio sorbents and other adsorbents. *Bioresource Technology* **160**, 142–149. https://doi.org/10.1016/j.biortech.2014.01.012.

Yang, H. J., Sun, L., Zhai, J. L., Li, H. Y., Zhao, Y. & Yu, H. W. 2014 In situ controllable synthesis of magnetic Prussian blue/graphene oxide nanocomposites for removal of radioactive cesium in water. *Journal of Materials Chemistry A* **2**, 326–332.

Yang, H. M., Jang, S. C., Hong, S. B., Lee, K. W., Roh, C., Huh, Y. S. & Seo, B.-K. 2016 Prussian blue functionalized magnetic nanoclusters for the removal of radioactive cesium from water. *Journal of Alloys and Compounds* **657**, 387–393.

Yuan, G. D., Theng, B. K. G., Churchman, G. J. & Gates, W. P. 2013 *Clays and Clay Minerals for Pollution Control*, 2nd ed., Vol. 5, no. C. Elsevier Ltd. doi:10.1016/B978-0-08-098259-5.00021-4.

Zabulonov, Y., Kadoshnikov, V., Zadvernyuk, H., Melnychenko, T. & Molochko, V. 2021 Effect of the surface hydration of clay minerals on the adsorption of cesium and strontium from dilute solutions. *Adsorption* **27**(1), 41–48. doi:10.1007/s10450-020-00263-y.

First received 4 April 2023; accepted in revised form 2 August 2023. Available online 31 August 2023